CHALMERS
UNIVERSITY OF TECHNOLOGY

Quantification of Drag Change of Rough Surfaces by Submicron Resolution Long-Distance Micro-PTV

13th International Symposium on Particle Image Velocimetry – ISPIV 2019
Munich, Germany, July 22-24, 2019

Quantification of Drag Change of Rough Surfaces by Submicron Resolution Long-Distance Micro-PTV

Bercelay Niebles Atencio[1], Valery Chernoray[1*], Mikhail Tokarev[2]

[1] Chalmers University of Technology, M2, Fluid Dynamics, Gothenburg, Sweden

[2] Kutateladze Institute of Thermophysics, Novosibirsk, Russia

[*] valery.chernoray@chalmers.se

Abstract

One of the major questions in fluid mechanics is the prediction of the mean flow and turbulence structure of boundary layers over surfaces with different roughness types. The current paper shows a method to obtain the roughness function of different surface roughness by using a small-scale rig with rotating discs and long-distance microscopic PTV measurements in order to obtain submicron resolution inside the boundary layer of rotating disc flows. This rig has been designed and constructed for the optical measurements and consists of an electric motor driving the discs that are rotating inside of a 20-liter water tank. The PTV measurements are performed on surfaces with different degree of roughness and a smooth case. The rough cases correspond to two applications of a marine antifouling paint. The measurements are performed for two rotational speeds (300 and 600 RPM). Field mean velocity profiles are calculated by averaging vertical bins with 1 px width and every point of the mean velocity profile corresponds to 200 instant velocity values from 2000 image pairs. The wall shear stress for every rough case is determined from the torque and the wall shear stress for the smooth case disc with same diameter. The mean velocity profiles are plotted and the roughness function is directly obtained and compared with results from indirect methods using resolved CFD simulations and torque measurements in the same facility.

1 Introduction

In a multitude of situations both in the natural environment and in engineering applications, wall-bounded turbulent flows over roughness occur. Some examples are the wind over canopies of plants, ship and aircraft boundary layers. Considering the fact that surface roughness not only affects the near-wall mean velocity profile but also the resulting drag and heat transfer, a great deal of research has been carried out. For example Nikuradse (1933), Clauser (1954), Hama (1954), Raupach et al. (1991), Antonia and Krogstad (2001).

Characterizing the drag of a rough surface implies finding the velocity decrement caused by the frictional drag of the surface as a function of the roughness Reynolds number. This relationship is commonly known as a roughness function Clauser (1954) and is unique for any particular surface roughness geometry. Once the roughness function for a given rough surface is known, it can be used in a numerical code or similarity law analysis to predict the drag of any body covered with that roughness, Granville (1985).

The log-law for smooth and rough walls reads:

$$U^+ = \frac{1}{\kappa} ln(y^+) + B \tag{1}$$

and

$$U^+ = \frac{1}{\kappa} ln(y^+) + B + \Delta U^+ \tag{2}$$

The roughness function ΔU^+ depends on the roughness Reynolds number k^+, which is defined as the ratio of the roughness length scale k to the viscous length scale $\frac{\nu}{U_\tau}$. The latter is based on the kinematic viscosity

ν and the friction velocity U_τ, which depends in turn on the wall shear stress and the density of the fluid.

A number of different approaches have been developed to determine ΔU^+. However, there is not yet any common agreement on this issue, since there is no universal ΔU^+ that can be used for all the surfaces. Another difficulty resides in the proper specification of the so-called roughness length scale k for a given roughness geometry.

Direct methods and indirect methods can be used for the determination of the ΔU^+. In the direct method, the ΔU^+ is directly measured by subtracting the mean velocity profile in the log-region of the rough surface from the log-region of the smooth surface. The indirect methods imply determining the pressure drop or wall shear stress in a channel or pipe flow. Another indirect method implies measuring the torque on rotating discs. All these measurements are used together with boundary layer similarity laws to obtain ΔU^+.

Nikuradse (1933) was the first in using an indirect approach for reporting the relation of the resistance factor of pipes roughened with sand and the velocity distribution. However, his roughness function can also be expressed as a dependence of ΔU^+ and k^+. This dependency has been implemented nowadays in commercial CFD codes thanks to the work by Cebeci and Bradshaw (1977). They obtained a parametric roughness function that uses a shape parameter (C_s) which can be set to obtain the classical Nikuradse roughness function as shown in Figure 1, taken from Niebles Atencio and Chernoray (2019).

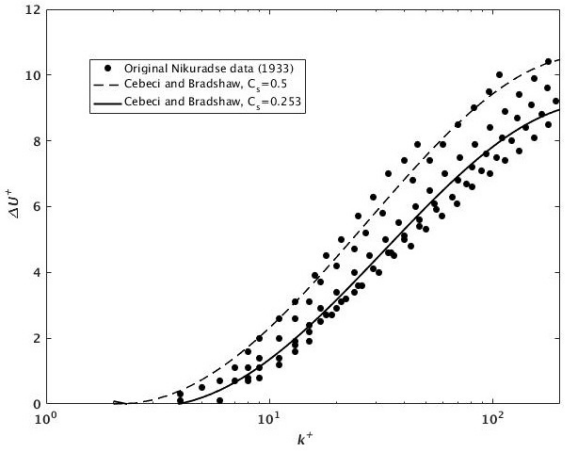

Figure 1: Cebeci and Bradshaw (1977) roughness function with two different shape parameters and Nikuradse (1933) data in terms of ΔU^+ and k^+.

The current paper presents several methods for obtaining the roughness function of any arbitrary rough surface by using different experimental approaches and a method utilizing resolved CFD RANS simulations. The drag characterization and the roughness function determination are performed for a smooth surface and two rough surfaces with different roughness shape and size. Long-distance microscopic PTV measurements are used in a rotating disc rig to obtain submicron resolution of the boundary layer of rough discs and determine ΔU^+. The roughness function obtained using long-distance micro-PTV is compared with the ΔU^+ resulting from an indirect method based on torque measurements in the same rotating disc rig with the same discs. Finally, the experimental approaches are also compared with the ΔU^+ that is determined from resolved CFD RANS simulations for the same roughnesses.

2 Experimental Methodology

In the current section, the rig used for the experiments and studied surfaces are described together with the experimental method.

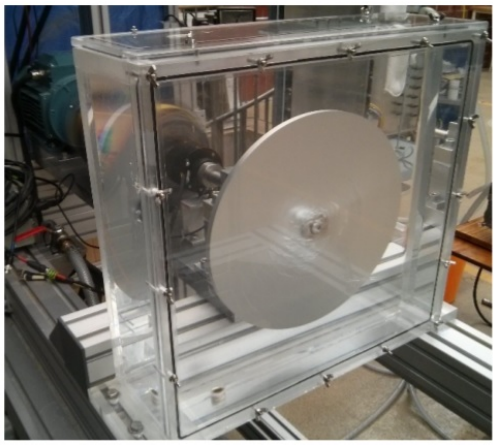

(a) Chalmers rotating disc rig for PTV measurements.

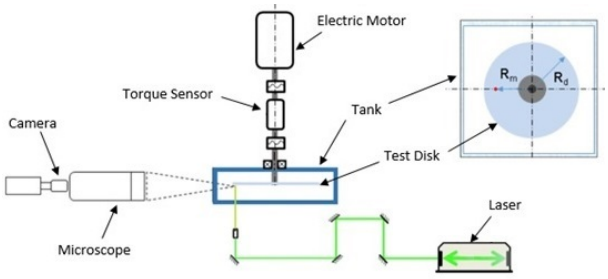

(b) Experimental setup sketch with all the components and the area on the disc where measurements were taken (red dot on the disc at the upper right).

Figure 2: Experimental setup

2.1 Experimental rig

A rotating disc rig has been designed and constructed for the measurements. The disc rotates by an electric motor in the middle of a 20-liter water tank. Figure 2 shows a picture and sketch of the measurement setup. Discs with radius r = 150 mm are used with different surface roughness. The PTV measurements are performed at a radius of 135 mm. The study includes a smooth reference and two different marine paint coatings. For each case, the measurements were performed at two different rotational Reynolds numbers equal to 5.7×10^5 and 1.15×10^6, corresponding to disk rotational speeds of 300 and 600 rpm, where the Reynolds number Re_r based on the rotational speed ω is defined as:

$$Re_r = \frac{r^2\omega}{\nu} \tag{3}$$

2.2 Test Surfaces

Two different types of rough surfaces are used that correspond to realistic surfaces of antifouling paints used in marine applications. At JOTUN A/S (Norway), models of discs have been prepared and scanned using 3D laser profilometry. These discs are tested in experimental rigs at Chalmers University of Technology (Sweden). The 3D profilometer surface scans are used as an input geometry for resolved CFD calculations. The method to obtain the coatings with different roughness is explained in detail in Savio et al. (2015). The discs were grinded, cleaned and degreased to enhance adhesion. The coating applications are made by airless spraying of the surfaces to give two levels of roughness A and B. Level A roughness simulates an optimal newly built ship or full blast dry docking paint application and the second level (B) of roughness, represents a poorly applied coating.

	Smooth	A	B
Disc 1	$0.62^{+12\%}_{-12\%}$	$14^{+6\%}_{-7\%}$	$35^{25\%}_{-13\%}$
Disc 2	$0.84^{+19\%}_{-13\%}$	$14^{+14\%}_{-12\%}$	$38^{24\%}_{-10\%}$
CFD	0	18	37

Table 1: Roughness data for painted discs and CFD simulations

The test discs have been scanned by R&D Chemists from JOTUN using a 3D laser profilometer. For the discs, the scanning is performed at four locations on each disc and two discs of each roughness type (A and B) were prepared. In addition, for the flat plates, the scanning is complemented by stylus measurements with the TQC DC9000 hull roughness analyser. The average roughness characteristics for different surfaces are

summarized in Table 1. The deviations show the upper and lower bounds from the different measurement locations. The profilometer scanning resulted in data files with coordinates XYZ that are used for creating CFD domains.

2.3 Micro-PTV measurements

The boundary layer profiles on discs is challenging to measure because of the very small thickness of the boundary layer (3-5 mm). Therefore, in order to determine the azimuthal velocity components near the discs wall with the high spatial resolution and to capture the inner layer of the turbulent boundary layer, a microscopic optics has been used. A long distance Questar QM1 microscope has been placed at a distance of 560 mm from the point of measurement, as shown in Fig. 2. The optical magnification is M = 4-12 times, so that the 1.5-4 mm area of interest was projected on a 16-mm camera image sensor. The minimal depth-of-field is of 155 μm, which defines the spatial resolution of the method. The microscope is the Maksutov Cassegrain Catadioptric type with two mirrors and had the f-number $\#f$ = 8.7 for the used configuration of optics.

Spherical PMMA particles (Microparticles GmbH) with the minimum diameter 1 μm are used for flow seeding. The particle density 1.19 g/cm^3 is close to the water density and the particles are small enough to follow the flow faithfully. The illumination is performed by a pulsed double-cavity Nd:YAG 532-nm laser with the pulse energy of 200 mJ (Quantel EverGreen EVG00200), and pulse duration less than 10 ns. The time separation between pulses of laser is 6-20 μs to keep relatively the same particle displacement in the images between different cases. The transferred and magnified scattering field of the flow with tracers has been registered by a monochrome double-frame CCD camera ImagerProX 4M (LaVision GmbH) with 2048 pixel by 2048 pixel resolution, 14-bit pixel depth, and 7.4-μm pixel size. The camera recording time is synchronized with the specific angle of rotation of the test disc through a signal from a Hall sensor. For the rotation speed 600 rpm, the camera registers image pairs every second revolution as its maximum frame rate at full resolution in double frame mode is 8.2 fps. Images have been registered with particle images in the form of a diffraction pattern with a central circular part and several rings around it as shown in Fig. 3. The

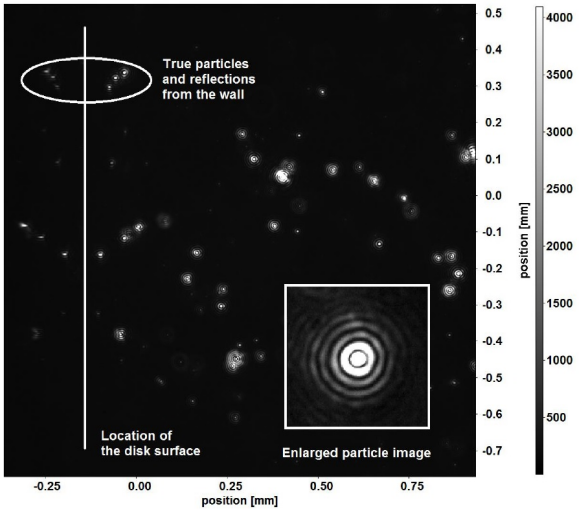

Figure 3: Example of images of registered light scattering signal from the particles and their reflections by the wall

particle image size is near 8 pixels in diameter. DaVis 8.2.2 software (LaVision GmbH) is used for data acquisition during the experiment. Geometrical calibration of the measurement field has been done by a metal wire with a known diameter 0.85 mm which is imaged in the measurement area before the actual experiment.

One of the important issues is the localization of the wall position in the images. For this purpose, a 10 mm radial transparent insert made of PMMA plastic is embedded in the disc as shown in Fig. 4 to provide a reflective surface. Another purpose of this insert is to reduce excessive light scattering from the rough surface that decreases the signal to noise ratio of particle images near the surface. The wall location is determined by reflections of the tracers near the wall as shown in Fig 3. The wall location is carefully ad-

justed parallel to the vertical image coordinate before the experiments to simplify the image processing. A camera recording synchronization with the specific angle of the test disc rotation is performed to carry out the measurements at fixed angular disc position and to freeze the disc at one position in a recording image. For data processing, a tracking based approach has been used with the identification of individual particle

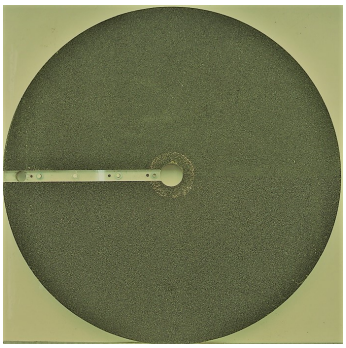

Figure 4: Example of a test disc with PMMA insert installed

images in both recorded image pairs and finding the correspondence between them. The particle image tracking is complicated by the large diffraction pattern size with the bright multiple rings, parts of which are identified as separate standalone particles with the standard available algorithms for the PTV method. In order to decrease this multiple identification, the raw images are pre-processed by correlating them with the Airy diffraction disc template intensity distribution, which is extracted from one of the recorded images. Example of the templates that has been used is shown in Fig. 5. According to the tests, the real particle image templates as one shown in Fig 5(b) gave better results for the particle identification efficiency. An

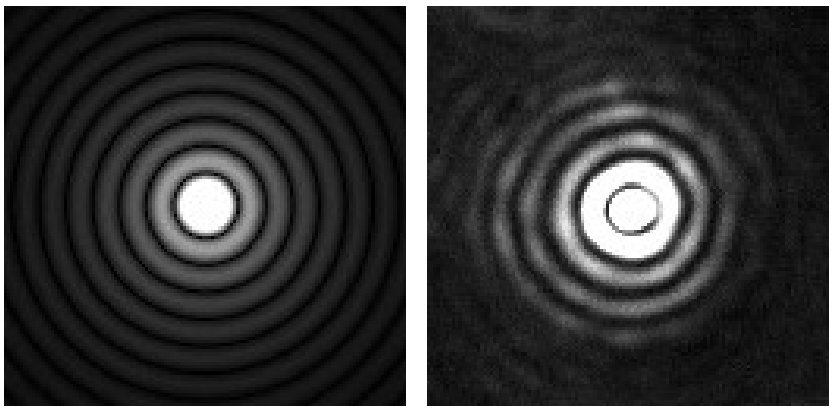

(a) Analytic template

(b) Real diffraction template from recorded image

Figure 5: Correlation templates for particle identification.

example of the normalized correlation of the experimental image with the template from Fig.5(b) and obtained vector field of the particles is presented in Fig. 6 . As can be seen the applied image pre-processing equalizes the intensity of the particle images regardless their original brightness and size, which helps to identify more objects and decrease the number of erroneous identifications linked with multiple rings in the Airy diffraction pattern. The particle concentration on the images is of the order of 5×10^{-5} particles per squared pixels px^2. The mean distance between neighboring tracers is approximately 150 px. A relatively simple nearest neighbor algorithm for a corresponding particle search in both frames is used, because the maximum possible displacement does not exceed 50 px or one third of the mean distance between particles for the mentioned particle concentration. Particles without a pair in one of the frames are rejected. Final mean velocity profiles are calculated by averaging vertical bins with 1 px width. Every point of a velocity profile is based upon near 200 instant velocity values obtained from 2000 PTV image pairs by using particle

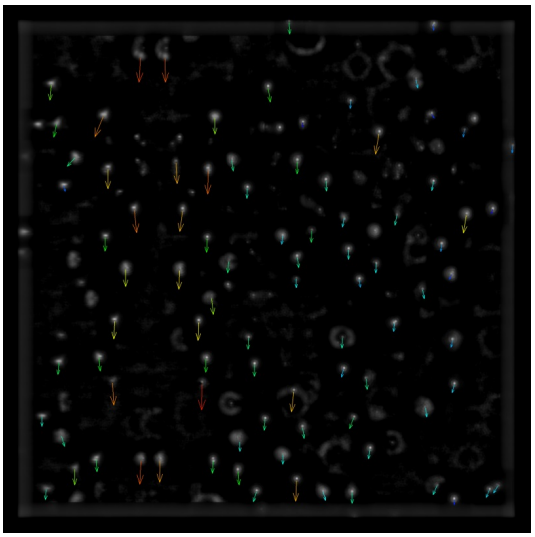

Figure 6: Pre-processed particle image by the normalized correlation with real diffraction patterns.

tracking approach described above.

The accuracy of the particle identification algorithm is 0.5 px due to the relatively large particle diameter, which is 8 px. Hence, for two identifications of start and end positions, the accuracy of an obtained particle displacement is determined as 1 px. This equals 4.3% at the region with the half disc velocity or absolute errors 0.18m/s and 0.36m/s for the disc rotational speeds of 300 and 600 rpm. The accuracy of the obtained mean velocity profile is 0.5% for the same region.

2.4 Torque Measurements

The torque or resisting moment has been measured for all the rough discs cases in order to obtain the wall shear stress. The Kistler type 4503A torque meter has been installed on the rig and measured torques of discs for rotational velocities from 0 to 600 RPM. First the torque of the shaft and bearings with seals is measured without a disc and these readings are then subtracted from the measured total torque in order to obtain the torque of the discs. The complete procedure for measuring the torque is explained in Niebles Atencio et al. (2016) and the procedure for indirectly determining the ΔU^+ values from torque measurements is explained with great detail in Niebles Atencio and Chernoray (2019) and Granville (1972).

3 Numerical Methodology by Resolved CFD Simulations

The governing equations of mass and momentum conservation have been solved in order to evaluate the drag caused by the roughness in a channel flow setup. The governing equations are discretized by the finite volume method and the governing equations are solved in the form of Unsteady Reynolds-Average Navier-Stokes equations (URANS) by using the k-ω SST turbulence model. Star-CCM + v 9.06.009 is the commercial CFD software used for this purpose.

The discs are scanned as mentioned in subsection 2.2 and the data obtained from that scanning is used to create STL files in Matlab from the contour of the surfaces as seen in Fig.7. Those surfaces are then exported into Ansys ICEM software to create the channel geometries and then for meshing the domain. A mesh independence study is carried out to find the most suitable mesh resolution. The meshes are then exported into Star-CCM+ for setting the boundary conditions, running the simulations and post-processing of the results. The complete setup procedure of the numerical simulations and post-processing for obtaining ΔU^+ is explained in great detail in Niebles Atencio and Chernoray (2019).

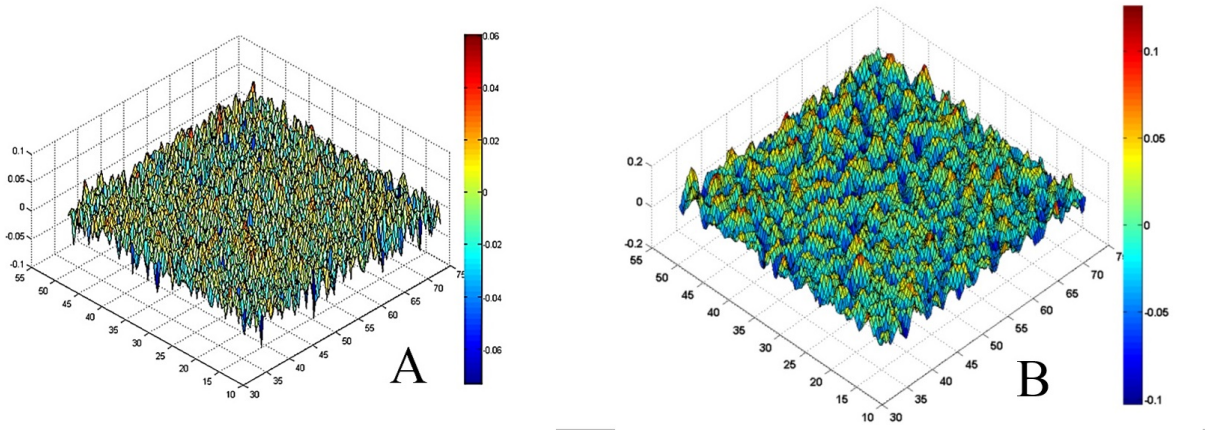

Figure 7: Contour plots from the scanning of the rough disc surfaces

4 Results

The determination of the wall shear stress on smooth disc for different Re_r has been carried out in previous tests by applying the method described in Clauser (1956) . This is done in order to obtain the required wall shear stress for the rough discs due to the fact that the skin friction coefficient increases in the same proportion than the torque for discs with same radius (Granville, 1972). The spacial distribution of the mean velocities are determined during the PTV post-processing. Together with the wall shear stresses determined from the proportionality of the torques for smooth and the rough cases, the law of the wall (Eq. 1) is applied to plot the different cases. In Eq. 1 and 2, the von Kármán constant is κ=0.41 and B=5.1.

A near-wall region of the smooth case velocity profile at 300 RPM is shown in Figure 8(a). As seen, the submicron resolution measurements allow resolving the viscous sublayer down to y^+=2 in a very thin turbulent boundary layer (5 mm thickness).

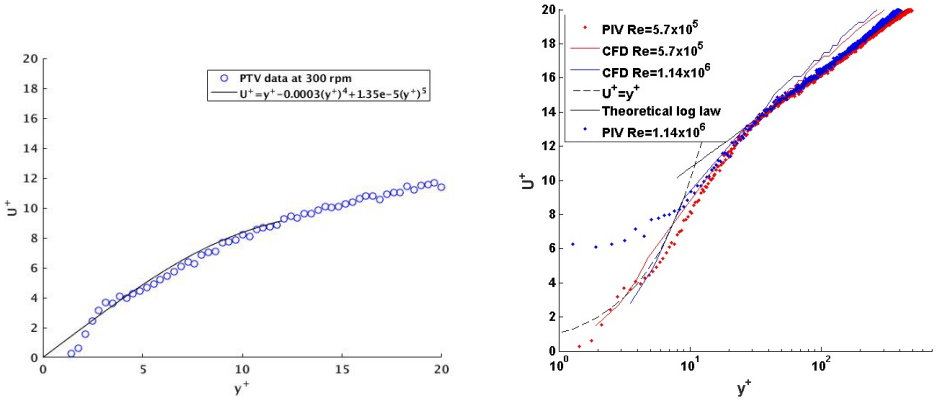

(a) Viscous sublayer region velocity profile from PTV measurements compared with theoretical mean velocity profile

(b) Entire velocity profile for the smooth case

Figure 8: Boundary layer measurements from micro-PTV and comparison to the theory and CFD.

Figure 8(b) shows the measured boundary layer velocity profile for the smooth disc for both Re_r. The mean velocity profiles from the PTV are compared with the theoretical law of the wall, according to Eq. 1 and with CFD simulations for smooth case. As the figure shows, the profiles from PTV agrees quite well

with the smooth theoretical line and the CFD computations in the log-region. Some high values of velocity are observed for the high Re_r case, which might indicate that the particles at those positions were not completely still and had some relative motion with respect to the disc surface.

In Figure 9, the logarithmic region ($30 < y^+ < 1000$) of the velocity profiles from micro-PTV measurements on rotating discs at 600 RPM is shown. The disc edge velocity relative to the bulk of the fluid for that rotational speed is of 9.4 m/s, if the swirl factor is taken into account as mentioned in Niebles Atencio and Chernoray (2019). The symbols show measured data for a reference smooth disc and for rough discs of Case A and B. The lines depict the offset predicted by the roughness functions from torque-based experimental method and from resolved RANS CFD. A very good consistency of both experimental approaches and good prediction by CFD can be observed. It can be noted that for Case A, the logarithmic velocity region is established at $y^+ > 400$ and for Case B at $y^+ > 200$. The agreement between the three methods is particularly good for the smallest roughness case, Case A. For Case B the agreement is still very good and a discrepancy in ΔU^+ is 0.5 counts.

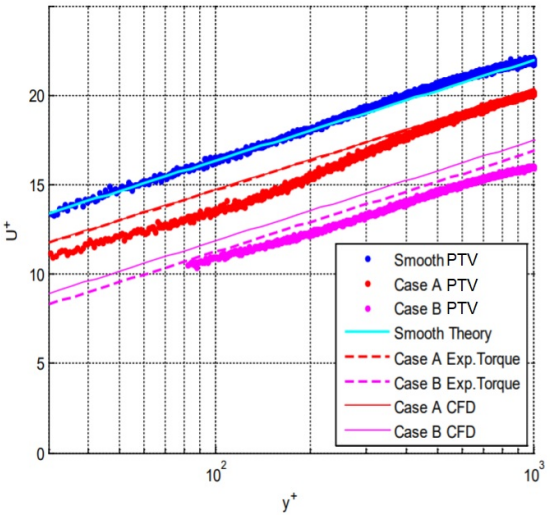

Figure 9: Log-region of velocity profiles from micro-PTV measurements on rotating disc at 600 RPM, compared with CFD and torque measurements

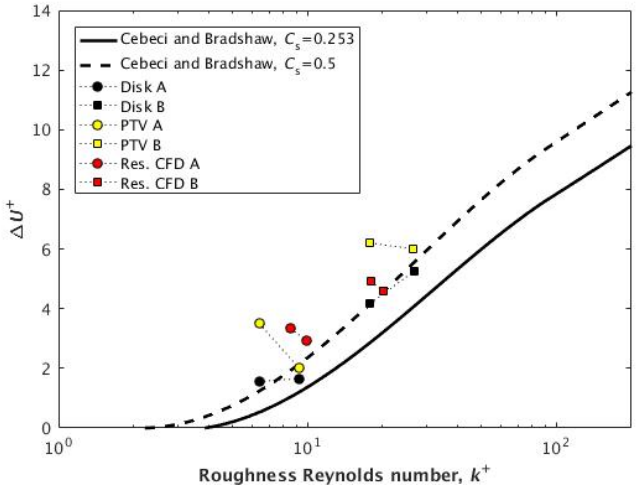

Figure 10: Comparison of roughness functions obtained from micro-PTV velocity profiles, indirect torque method and CFD.

The quantification of the drag for rough surfaces (i.e, the values of ΔU^+) is commonly plotted against the k^+ as in Fig. 10. The roughness function from experimental data in the rotating disc facility and CFD simulations are shown for different values of k^+ in the figure. The Cebeci and Bradshaw (1977) roughness function (which is implemented in CFD commercial software) is shown for comparison. This particular roughness function provides very good drag predictions for all studied roughness cases A and B when the root mean square height R_q is used as the roughness height. There are two sets of experimental data shown in Fig. 10, one obtained from torque measurements and one obtained from PTV velocity profiles. It is seen from this figure that the PTV results at rotational speed 600 RPM (data points in each set having larger values of k^+)agree well with the results from torque measurements and CFD. The agreement is reduced, however, for lower rotational speeds because the boundary layer profiles are possibly not fully developed.

5 Conclusion

Long-distance micro-PTV measurements in the boundary layer of rotating flow over discs with different surface roughness have been performed. The results presented show that by using micro-PTV, the mean velocity profile in turbulent boundary layers can be determined with a sub-micrometer resolution.

The wall shear stress can also be determined with enough accuracy for a smooth disc using micro-PTV measurements. From the smooth wall shear stress, the wall shear stress for rough discs can be obtained by using the torque data for the rough discs.

The roughness functions that are obtained with micro-PTV can be compared with values from resolved CFD simulations and values from torque measurements for the same discs. The low speed case with micro-PTV gives the least agreement with respect to the other methods.

In general, this paper shows that along with the other techniques, it is possible to directly determine the roughness function for any arbitrary rough surface by using particle based optical tracking velocimetry.

Acknowledgements

The experiments were performed on resources provided by the Chalmers Laboratory of Fluids and Thermal Sciences. The simulations were performed on resources provided by the Swedish National Infrastructure for Computing (SNIC).

References

Antonia RA and Krogstad PÅ (2001) Turbulence structure in boundary layers over different types of surface roughness. *Fluid Dynamics Research* 28:139–157

Cebeci T and Bradshaw P (1977) Momentum transfer in boundary layers pages 176–180

Clauser F (1954) Turbulent boundary layers in adverse pressure gradients. *Journal of the Aeronautical Sciences* 21:91–108

Clauser F (1956) The turbulent boundary layer. *Adv Appl Mech* 4:1–51

Granville P (1972) The torque and turbulent boundary layer of rotating discs with smooth and rough surfaces, and in drag-reducing polymer solutions. *Report 3711, Dept of the Navy Naval Ship Res and Dev Center*

Granville P (1985) Mixing-length formulations for turbulent boundary layers over arbitrary rough surfaces. *J Ship Res* 29:223–233

Hama F (1954) Boundary-layer characteristics for rough and smooth surfaces.. *Trans SNAME* 62:333–351

Niebles Atencio B and Chernoray V (2019) A resolved RANS CFD approach for drag characterization of antifouling paints. *Ocean Engineering* 171:519–532

Niebles Atencio B, Tokarev M, and Chernoray V (2016) Submicron resolution long-distance micro-piv measurements in a rough-wall boundary layer. *Proc of 18th International Symposia on Applications of Laser Techniques to Fluid Mechanics*

Nikuradse J (1933) Laws of flow in rough pipes. *NACA TM 1292*

Raupach M, Antonia R, and Rajagopalan S (1991) Rough-wall turbulent boundary layers. *Appl Mech Rev* 44:1–25

Savio L, Ola B, Koushan K, and Axelsson M (2015) Measurements of added resistance due to increased roughness on flat plates. *AMT 2015 Conference, Istanbul*